

Area Rate Efficiency in Molecular Communications

Lukas Brand^{*}, Sebastian Lotter^{*}, Vahid Jamali[†], and Robert Schober^{*}

^{*}Friedrich-Alexander University, Erlangen-Nuremberg, Germany

[†]Princeton University, Princeton, United States

lukas.brand@fau.de,sebastian.g.lotter@fau.de,jamali@princeton.edu,robert.schober@fau.de

ABSTRACT

We consider a multiuser diffusion-based molecular communication (MC) system where multiple spatially distributed transmitter (TX)-receiver (RX) pairs establish point-to-point communication links employing the same type of signaling molecules. To realize the full potential of such a system, an in-depth understanding of the interplay between the spatial user density and inter-user interference (IUI) and its impact on system performance in an asymptotic regime with large numbers of users is needed. In this paper, we adopt a three-dimensional (3-D) system model with multiple independent and spatially distributed point-to-point transmission links, where both the TXs and RXs are positioned according to a regular hexagonal grid, respectively. Based on this model, we first derive an expression for the channel impulse responses (CIRs) of all TX-RX links in the system. Then, we provide the maximum likelihood (ML) decision rule for the RXs and show that it reduces to a threshold-based detector. We derive an analytical expression for the corresponding detection threshold which depends on the statistics of the MC channel and the statistics of the IUI. Furthermore, we derive an analytical expression for the bit error rate (BER) and the achievable rate of a single transmission link. Finally, we propose a new performance metric, which we refer to as area rate efficiency (ARE), that captures the tradeoff between the user density and IUI. The ARE characterizes how efficiently given TX and RX areas are used for information transmission and is given in terms of bits per area unit. We show that there exists an optimal user density for maximization of the ARE. Results from particle-based and Monte Carlo simulations validate the accuracy of the expressions derived for the CIR, optimal detection threshold, BER, and ARE.

1 INTRODUCTION

In molecular communication (MC), molecules are used to convey information. Possible industrial applications of MC can be envisioned in bio-inspired robotics to improve search and rescue operations, in agriculture to understand and potentially control animal behavior, and in the oil and gas industry [5]. In general, the data rate in MC is low compared to conventional communication systems, which are based on electromagnetic waves. Furthermore, the particularities of MC are often investigated for MC systems which involve only a single transmission link, i.e., one transmitter (TX) node that releases molecules and one receiver (RX) node that counts the received molecules. However, for practical applications, high data rates and large numbers of transmission links are desired. A common approach to increase the throughput of MC systems is to decrease the symbol duration, which leads to inter-symbol interference (ISI) [13, 14, 16].

Besides the time dimension, the spatial dimension can also be exploited to increase the system throughput, which has received less attention. Existing works investigate the spatial dimension for

example in the context of multiple-input multiple-output (MIMO) MC systems [3, 6, 7, 11, 11, 15] or for large-scale MC systems with many transmission nodes exploiting tools from three-dimensional (3-D) stochastic geometry [4]. An MC MIMO system comprises one TX and one RX, but the TX and the RX are connected to multiple spatially distributed release and reception sites, respectively. Hence, well known techniques such as spatial modulation for encoding [6, 7], and selection combining and zero forcing for decoding [11, 15] are applicable. Performance benefits of MIMO MC systems, such as diversity gain and spatial multiplexing gain, are discussed in [3, 11]. In all existing studies on MIMO MC systems, the considered number of release/reception sites is quite low. To the best of the authors' knowledge, the largest such system was investigated in [6], which studied an 8×8 system. Unlike the studies on MC MIMO, a large-scale MC system with an asymptotically large number of transmitters is investigated in [4]. There, a swarm of randomly placed transmitters simultaneously transmit *the same bit sequence* to one receiver. Methods from stochastic geometry are utilized to derive the resulting received signal and the corresponding bit error rate (BER).

In order to gain a fundamental understanding of the benefits of exploiting the spatial dimension in MC, in this paper, we study an MC system with a large number of *independent* users, i.e., an asymptotic regime in terms of the number of TX and RX nodes. We raise the following research question: **For given transmit and receive areas, in which the TXs and RXs can be placed, how dense should the TXs and RXs be deployed to maximize the information transmission rate?** Similar to other resources such as transmission time, the spatial resource allocated to different users should be optimized. There exists a fundamental tradeoff between the achievable data rate of *one* TX-RX link, which we refer to as user rate, and the link density. Increasing the density of TXs and RXs increases the number of independent transmission links per area unit. We refer to the number of links per area unit as spatial multiplexing rate with unit $[1/m^2]$. However, the molecules released from different TXs may cause inter-user interference (IUI) at the RX units. Therefore, increasing the density of TXs and RXs increases the BER and consequently decreases the user rate.

In order to analyze the aforementioned tradeoff, we propose a new performance metric for MC systems which we refer to as area rate efficiency (ARE). The ARE is the product of the spatial multiplexing rate and the user rate and characterizes how efficiently a given area is used for information transmission and is given in terms of bits per area unit. To systematically address the question posed above, the following communication system is considered and evaluated.

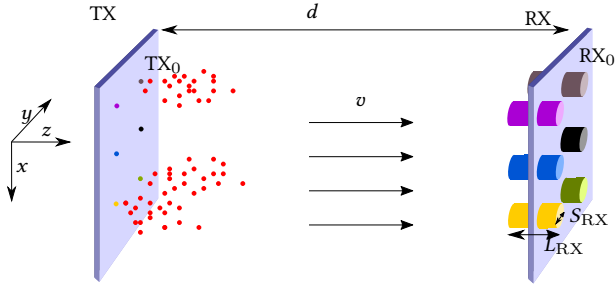


Figure 1: Unbounded system model with multiple, independent point-to-point transmission links (highlighted by different colors). The point TXs are aligned within a predefined grid on a virtual TX plane, shown in blue on the left, and release molecules (red dots) using ON-OFF keying (OOK). The molecules propagate by Brownian motion and directed flow and are detected by transparent volume RXs which are aligned on a virtual RX plane, depicted in blue on the right, on the same grid as the TXs.

We study a 3-D multipoint-to-multipoint communication system comprising multiple independent, spatially distributed point-to-point transmission links and analyze the system in the asymptotic regime with a large number of users. As in conventional wireless communications [2, 12], we define a location model for the positions of the TXs and RXs in the considered multi-link MC setup, i.e., a fixed and predefined cellular structure. Furthermore, we assume that every TX has exactly one RX as desired communication partner. We evaluate the performance of the considered system by deriving an analytical expression for the ARE. The main contributions of this work include:

- (1) An analytical expression for the channel impulse responses (CIRs) of all TX-RX links for multipoint-to-multipoint molecule transmission via diffusion and directed flow is derived assuming point TXs and transparent RXs with cylindrical volume.
- (2) Based on the CIR, mathematical expressions for the optimal detection threshold of a threshold detector, the BER, the user rate, the spatial multiplexing rate, and finally the ARE are derived in the asymptotic regime for large numbers of users.
- (3) By analyzing the ARE, we demonstrate a fundamental trade-off between the spatial multiplexing rate and the IUI dependent user rate on the overall performance of the considered multipoint-to-multipoint transmission system. Our analysis shows that there exists an optimal number of transmission links per space unit which maximizes the ARE.

The remainder of this work is organized as follows. Section 2 introduces the system model. In Section 3, the CIR and the statistics of the IUI are derived. The considered threshold detector and the performance metrics, namely the BER and the ARE, are analyzed in Section 4, and quantitatively studied and compared to particle-based and Monte Carlo simulations in Section 5. Finally, Section 6 concludes this work.

2 SYSTEM MODEL

We consider a 3-D MC environment with an infinite number of point TXs and an infinite number of transparent RXs, see Fig. 1. The TXs are confined to a plane at $z = z_0$ and the RXs are placed

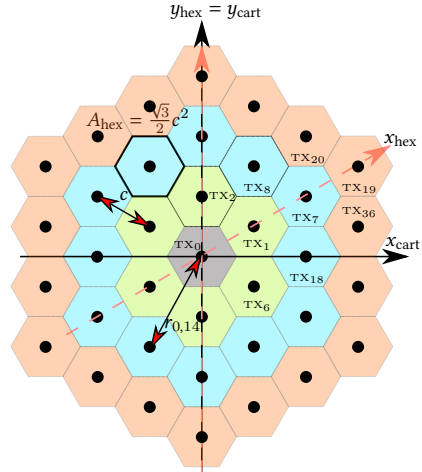


Figure 2: The point release positions are denoted as black dots within the virtual hexagonal grid with axes x_{hex} and y_{hex} ; the axes of the Cartesian coordinate system x_{cart} and y_{cart} are included as a reference. The distance c between two adjacent TXs as well as the exemplary distance $r_{0,14}$ between the reference TX in the center and TX_{14} are depicted by arrows. Multiple TXs having a similar distance to RX_0 align to rings of interferers which is highlighted with the same grid fill color, e.g., $\text{TX}_1 - \text{TX}_6$ are in the green cells, $\text{TX}_7 - \text{TX}_{18}$ in the blue cells, and $\text{TX}_{19} - \text{TX}_{36}$ in the orange cells.

in a plane at $z = z_R$. Both planes are virtual, i.e., are insubstantial, have infinite width and height, i.e., are infinite in x and y direction, and are separated by distance d . In the following, these planes are referred to as TX-plane and RX-plane, respectively. Each TX in the TX-plane is paired with the closest RX in the RX-plane, i.e., each TX wants to communicate with only one RX. We assume that TX-plane and RX-plane are subdivided into an infinite number of hexagons, resulting in a hexagonal grid. The hexagonal grid is widely used for analyzing cellular architectures, e.g., in wireless communication networks [2, 12]. Furthermore, hexagons are the closest shape to a circle that can still form a continuous grid, and therefore, guarantee the densest cellular packing. Each point TX and the center of each RX are in the center of a hexagon. The TX and RX hexagonal grids consist of regular, equally sized hexagons. The center points of the hexagons can be given in terms of an offset coordinate system x', y' and are identical for the TX plane and the RX plane. The Euclidean distance between the center points of two adjacent cells is given by c . For general center points, the distance to $(x', y') = (0, 0)$ is $c \sqrt{x'^2 + y'^2 + x' y'}$. The offset coordinate system x', y' is related to the Cartesian coordinate system x, y by $x = c \frac{\sqrt{3}}{2} x', y = c (y' + \frac{1}{2} x')$. The area of one hexagon is given by $A_{\text{hex}} = \frac{\sqrt{3}}{2} c^2$. The hexagonal grid structure is depicted in Fig. 2. The considered arrangement ensures that for each TX, the paired RX has the shortest distance to it and that this distance is equal for all TX-RX pairs. We index the TXs and RXs as TX_i and RX_j with $i \in [0, N_{\text{TX}} - 1]$ and $j \in [0, N_{\text{RX}} - 1]$, where $N_{\text{TX}} \rightarrow \infty$ and $N_{\text{RX}} \rightarrow \infty$, respectively. We note that the number of TXs is equal to the number of RXs, i.e., $N_{\text{TX}} = N_{\text{RX}}$. Without loss of

generality (w.l.o.g.) in this and the following sections, the analysis is done exemplary for the point-to-point transmission link between TX₀ and RX₀, which are at the center of the x - y plane, i.e., the center points are $(x_{\text{TX}_0}, y_{\text{TX}_0}) = (x_{\text{RX}_0}, y_{\text{RX}_0}) = (0, 0)$, see Fig. 2. All other TXs, i.e., TX₁, TX₂, ..., TX_{N_{TX}-1}, act as interferers to TX₀. All results are valid as well for the other TX-RX pairs due to the symmetry of the considered grids and the infinite extent of the TX- and RX-planes. We note that practical MC systems will have finite dimensions, of course. However, considering a system with infinite dimensions is needed to gain fundamental insights for system design. Furthermore, considering infinite dimensions provides an upper bound on the IUI for system models with a finite number of TXs and RXs as it constitutes the worst case scenario in terms of IUI.

At the beginning of each symbol interval, each point TX_{*i*} releases a fixed non-zero number of molecules, N_m , or zero molecules, representing binary symbols $s_i = 1$ and $s_i = 0$, respectively, i.e., the TXs use ON-OFF keying (OOK) modulation [8]. We assume that the binary values 0 and 1 are equiprobable, i.e., $\Pr\{s_i = 1\} = 0.5 = \Pr\{s_i = 0\}$. All molecules considered in this setup are of the same type. The symbol intervals are synchronized between the TXs, i.e., the TXs transmit at the same time instants. We assume that the release, propagation, and reception of all molecules are independent from each other. The movement of the released molecules from the TXs to the RXs is affected by diffusion and a uniform flow in z direction with velocity $v = v_z$. We neglect additional effects due to external forces, degradation, and interactions between molecules. Each RX counts the number of molecules within its volume at a fixed sampling time t_s , i.e., we consider transparent RXs in this work. The sampling time t_s at RX₀ is chosen such that it coincides with the time instant where the CIR between TX₀ and RX₀ has its peak. All RXs have the same size and a cylindrical shape, and can be characterized in terms of their radius S_{RX} and length L_{RX} . We chose cylindrical receivers as this enables an independent scaling of the receiver size in the xy -plane via S_{RX} and the z -axis via L_{RX} . The observed number of molecules, r , within RX₀ comprises the molecules originating from TX₀, c_s , and molecules received from other TXs, c_{IUI} , which constitute IUI. Hence, the received number of molecules at the sampling time at RX₀ is given by

$$r = c_s + c_{\text{IUI}}. \quad (1)$$

We note that multiple consecutive emissions of molecules may cause ISI if the symbol duration is too short. However, since the focus of this paper is the spatial dimension, we assume that ISI is negligible which is a valid assumption if the symbol duration is sufficiently large.

3 ANALYTICAL CHANNEL MODEL

In this section, we first derive an expression for the CIRs of all transmission links that involve receiver RX₀. We note that the derived CIR expression is also valid for all other TX-RX pairs due to the considered symmetric system model. Next, we analyze the distributions of the information and the interfering molecules.

3.1 Channel Impulse Response

We consider an unbounded environment with constant advection along the z -axis with velocity $v = v_z$ and diffusion coefficient D . We derive the expected number of molecules observed at RX₀

normalized to the instantaneous release of one molecule by TX_{*i*} at position $\mathbf{p}_{0,i} = (x_{0,i}, y_{0,i}, z_{0,i})$ and time $t_{0,i} = 0$ as a function of time, which we refer to as CIR. In the following proposition, we provide an analytical expression for the CIR in terms of an infinite sum.

PROPOSITION 1. *The expected number of particles at the cylindrical and transparent receiver RX₀ with dimensions $0 \leq r = \sqrt{x^2 + y^2} \leq S_{\text{RX}}$, $0 \leq \varphi < 2\pi$, and $z_S < z < z_E$, due to the release of one molecule at transmitter TX_{*i*} is given by*

$$\text{CIR}_{i,0}(t) = \frac{1}{2} \left(\text{erf} \left(\frac{z_0 + vt - z_S}{\sqrt{4Dt}} \right) - \text{erf} \left(\frac{z_0 + vt - z_E}{\sqrt{4Dt}} \right) \right) \times e^{-\frac{r_{0,i}^2}{4Dt}} \sum_{k=0}^{k_{\text{max}}=\infty} \frac{\left(\frac{r_{0,i}^2}{4Dt}\right)^k}{(k!)^2} \gamma(k+1, \frac{S_{\text{RX}}^2}{4Dt}), \quad (2)$$

where $r_{0,i}^2 = x_{0,i}^2 + y_{0,i}^2$. Here, φ denotes the angle in the xy -plane in relation to the positive x -axis. Furthermore, $\text{erf}(x)$, $I_0(x)$, and $\gamma(a, x)$ denote the Gaussian error function, the zeroth order modified Bessel function of the first kind, and the lower incomplete Gamma function, respectively.

PROOF. The molecule concentration $C(x, x_{0,i}, y, y_{0,i}, z, z_{0,i}, t, t_{0,i})$ for the case considered in Proposition 1 is given in [8, eq. (18)]. $C(x, x_{0,i}, y, y_{0,i}, z, z_{0,i}, t, t_{0,i})$ can be transformed to a cylindrical coordinate system by $x = r \cos(\varphi)$, $y = r \sin(\varphi)$, $x_{0,i} = r_{0,i} \cos(\varphi_{0,i})$, $y_{0,i} = r_{0,i} \sin(\varphi_{0,i})$, $z = z$. Assuming $t_{0,i} = 0$ and noting that $z_{0,i} = z_0$ is valid for all TXs, we obtain:

$$C_c(r, r_{0,i}, \varphi, \varphi_{0,i}, z, z_0, t) = \frac{1}{(4\pi Dt)^{3/2}} \times \exp \left(-\frac{r^2 + r_{0,i}^2 - 2r_{0,i}r \cos(\varphi - \varphi_{0,i}) + (z - z_0 - vt)^2}{4Dt} \right). \quad (3)$$

Furthermore, since the center of the circular cross section of the receiver is located at $r = 0$, the expected number of counted particles is obtained as

$$\begin{aligned} \text{CIR}_{i,0}(t) &= \int_0^{S_{\text{RX}}} \int_0^{2\pi} \int_{z=z_S}^{z_E} C_c(r, r_{0,i}, \varphi, \varphi_{0,i}, z, z_0, t) r \, dz \, d\varphi \, dr \\ &\stackrel{(a)}{=} \frac{1}{4Dt} \left(\text{erf} \left(\frac{z_0 + vt - z_S}{\sqrt{4Dt}} \right) - \text{erf} \left(\frac{z_0 + vt - z_E}{\sqrt{4Dt}} \right) \right) \\ &\quad \times \int_0^{S_{\text{RX}}} I_0 \left(\frac{r_{0,i}r}{2Dt} \right) \exp \left(-\frac{r^2 + r_{0,i}^2}{4Dt} \right) r \, dr \\ &\stackrel{(b)}{=} \frac{1}{4Dt} \left(\text{erf} \left(\frac{z_0 + vt - z_S}{\sqrt{4Dt}} \right) - \text{erf} \left(\frac{z_0 + vt - z_E}{\sqrt{4Dt}} \right) \right) \\ &\quad \times \exp \left(-\frac{r_{0,i}^2}{4Dt} \right) \int_0^{S_{\text{RX}}} \sum_{k=0}^{k_{\text{max}}=\infty} \exp \left(-\frac{r^2}{4Dt} \right) \frac{\left(\frac{r_{0,i}r}{4Dt}\right)^{2k}}{(k!)^2} r \, dr, \quad (4) \end{aligned}$$

where we exploited (a) $\text{erf}(x) = \frac{2}{\sqrt{\pi}} \int_0^x \exp(-y^2) \, dy$ and $I_0(x) = \frac{1}{\pi} \int_0^\pi \exp(x \cos(\varphi)) \, d\varphi$, and (b) the series expansion of $I_0(x)$ [1, eq. (9.6.10)], and $\gamma(a, x) = \int_0^x y^{a-1} \exp(-y) \, dy$ to obtain (2). \square

Eq. (2) shows that the expected number of particles received from different TXs depends on their release positions, characterized by $r_{0,i}$. All other parameters in (2), e.g., the z -position of the TXs, the

diffusion coefficient D and the flow velocity v are equal for all TXs. We note that, as will be shown in Section 5.2, the infinite sum over k in (2) can be truncated to a small number of terms (e.g., 20) without compromising its accuracy.

3.2 Statistical Model

We now describe the underlying models and associated distributions of c_s and c_{IUI} .

3.2.1 Information Molecules. Information carrying molecules intended for RX_0 are released for signaling $s_0 = 1$ at TX_0 . At time instant t_m , a corresponding particle is received with probability $\text{CIR}_{0,0}(t = t_m)$ at RX_0 . The expected (non-normalized) number of observed information molecules at sampling time t_s is given by $\bar{c}_s = N_m \text{CIR}_{0,0}(t_s)$. We statistically model the reception of the released particles by a Poisson distribution, i.e.,

$$c_s \sim \text{Pois}(s_0 \bar{c}_s) = f_s(c_s | s_0), \quad (5)$$

which is a valid approximation for typical MC scenarios [8]. Here, $f_s(c_s | s_0)$ denotes the distribution of c_s conditioned on s_0 .

3.2.2 Interference Molecules from other Transmitters. Besides the information molecules, molecules emitted by $\text{TX}_1, \text{TX}_2, \text{TX}_3, \dots, \text{TX}_{N_{\text{TX}}-1}$, i.e., TXs belonging to other TX-RX pairs, are received as IUI at RX_0 . These molecules are not distinguishable from the information molecules. Thereby, IUI degrades the detection of the signal from TX_0 at RX_0 [14]. We note that $\text{TX}_i, i \neq 0$, causes interference at RX_0 only for $s_i = 1$ as no molecules are released for $s_i = 0$. Hence, which of the interferers are active, i.e., send a 1, and the Brownian motion of the molecules both introduce randomness. So, for a complete analysis, all possible combinations of active TXs as well as the randomness and statistics of the molecule movement have to be taken into account.

From the perspective of RX_0 , the expected IUI at sampling time $t = t_s$ can be collected in vector $\bar{c}_{\text{IUI}} = [\bar{c}_1, \bar{c}_2, \dots, \bar{c}_{N_{\text{TX}}-1}]$ with $\bar{c}_i = N_m \text{CIR}_{i,0}(t = t_s)$. The received number of molecules from each interferer can be characterized by a Poisson distribution [8]. The molecule releases at the different TXs are independent of each other. As RX_0 counts all molecules independent of their origin, the sum over all Poisson distributed interfering molecules follows again a Poisson distribution, i.e.,

$$c_{\text{IUI}} \sim \text{Pois}(s_{\text{IUI}} \bar{c}_{\text{IUI}}^T) = f_{\text{IUI}}(c_{\text{IUI}} | s_{\text{IUI}}), \quad (6)$$

where $f_{\text{IUI}}(c_{\text{IUI}} | s_{\text{IUI}})$ denotes the distribution of c_{IUI} conditioned on vector $s_{\text{IUI}} = [s_1, s_2, \dots, s_{N_{\text{TX}}-1}]$, which contains the symbols emitted by the interfering TXs. There are $N_{\text{IUI}} = 2^{N_{\text{TX}}-1}$ possible realizations of s_{IUI} , i.e., different IUI states, which are equiprobable due to the equiprobable binary transmission symbols. Note that N_{IUI} grows exponentially in N_{TX} and we assumed $N_{\text{TX}} \rightarrow \infty$. However, we will later show numerically that the IUI can be accurately approximated by taking into account only a finite number of interfering TXs. The IUI is dominated by the strongest interferers, which correspond to the TXs nearest to TX_0 . From Fig. 2, it can be seen that the indexes of the TXs are chosen such that, for increasing index number, the distance between TX_0 and TX_i is monotonically non-decreasing in i . Therefore, the *strongest* interferers are always included if N_{TX} is truncated to a finite number. We note that the actual number of TXs necessary to accurately approximate the system behavior depends on the channel parameters, see Section 5.3.

4 SYMBOL DETECTION AND PERFORMANCE ANALYSIS

In this section, we first derive the optimal maximum likelihood (ML) decision rule and the BER of one TX-RX pair. Then, we provide the user rate defined as the achievable information transmission rate of an individual transmission link, and the spatial multiplexing rate which depends on the spatial density of the TX-RX pairs. Finally, we introduce the ARE to characterize the performance of the entire system.

4.1 Optimal ML Detector

For detection, we assume all CIRs in the system are known but the activity of the interfering TXs is only statistically known. Therefore, the ML estimate, \hat{s}_0 , is given by

$$\hat{s}_0 = \underset{s_0 \in \{0,1\}}{\text{argmax}} f_r(r | s_0) = \underset{s_0 \in \{0,1\}}{\text{argmax}} \mathbb{E}_{s_{\text{IUI}}} \{f_r(r | s_0, s_{\text{IUI}})\} \quad (7)$$

$$= \begin{cases} 1, & \text{if } \frac{\sum_{s_{\text{IUI}} \in M} \frac{(\bar{c}_s + s_{\text{IUI}} \bar{c}_{\text{IUI}}^T)^r e^{-(\bar{c}_s + s_{\text{IUI}} \bar{c}_{\text{IUI}}^T)}}{r!}}{\sum_{s_{\text{IUI}} \in M} \frac{(s_{\text{IUI}} \bar{c}_{\text{IUI}}^T)^r e^{-(s_{\text{IUI}} \bar{c}_{\text{IUI}}^T)}}{r!}} \geq 1 \\ 0, & \text{otherwise} \end{cases}, \quad (8)$$

where $f_r(r | s_0)$ denotes the distribution of r conditioned on s_0 , which is a Poisson distribution with mean $s_0 \bar{c}_s + s_{\text{IUI}} \bar{c}_{\text{IUI}}^T$ as both c_s and c_{IUI} are Poisson distributed, cf. (1). Here, $\mathbb{E}_{s_{\text{IUI}}}\{\cdot\}$ and $M = \{0, 1\}^{N_{\text{TX}}-1}$ denote the expectation over the IUI and the set of interference symbols, respectively. The ML detection in (8) is computationally complex as all possible realizations of the IUI have to be taken into account and has to be computed for every received r . Note that evaluating (8) is only feasible for a finite number of interferers, see Section 3.2.2. In the following, we show that (8) can be equivalently realized by a threshold detector employing a pre-calculated threshold. Threshold detection is preferable as the threshold for a given setup has to be computed only once offline and then can be used throughout the transmission. Therefore, the computational cost for online data detection is reduced.

THEOREM 1. *The ML detection problem given in (8) can be written equivalently as a threshold detection*

$$\hat{s}_0 = \begin{cases} 1, & \text{if } r \geq \xi \\ 0, & \text{otherwise} \end{cases} \quad (9)$$

with threshold value ξ obtained by

$$\xi = \min \left\{ \Theta \in \mathbb{N} \mid \sum_{s_{\text{IUI}} \in M} (\bar{c}_s + s_{\text{IUI}} \bar{c}_{\text{IUI}}^T)^\Theta e^{-(\bar{c}_s + s_{\text{IUI}} \bar{c}_{\text{IUI}}^T)} \geq \sum_{s_{\text{IUI}} \in M} (s_{\text{IUI}} \bar{c}_{\text{IUI}}^T)^\Theta e^{-(s_{\text{IUI}} \bar{c}_{\text{IUI}}^T)} \right\}. \quad (10)$$

PROOF. Due to space limitation, we provide only a sketch of the proof. The existence of a unique threshold level ξ can be proved by showing that the fraction in (8) is monotonically increasing in r , i.e., for low values of r , i.e., $r < \xi$, the fraction is always smaller than 1, and for large values of r , i.e., $r \geq \xi$, the fraction is always at least equal to 1. This can be proved using the same steps as in a similar proof in [9, Appendix]. \square

4.2 Bit Error Rate of one TX-RX Pair

The BER can be expressed as

$$P_e = \mathbb{E}_{s_0} \{ \mathbb{E}_{\mathbf{s}_{\text{IUI}}} \{ P_e(\hat{s}_0 | \mathbf{s}_{\text{IUI}}, s_0) \} \} \\ = \sum_{s_0} \sum_{\mathbf{s}_{\text{IUI}}} P_e(\hat{s}_0 | \mathbf{s}_{\text{IUI}}, s_0) f(\mathbf{s}_{\text{IUI}}) f(s_0), \quad (11)$$

where $P_e(\hat{s}_0 | \mathbf{s}_{\text{IUI}}, s_0)$ is the error probability conditioned on given transmitted symbol s_0 and interference vector \mathbf{s}_{IUI} . In the following, we derive the BER for the proposed threshold detector.

PROPOSITION 2. *For the proposed threshold detector, P_e can be expressed as*

$$P_e = \frac{1}{2} \frac{1}{N_{\text{IUI}}} \sum_{\mathbf{s}_{\text{IUI}} \in \mathcal{M}} \underbrace{Q(\xi, \bar{c}_s + \mathbf{s}_{\text{IUI}} \bar{\mathbf{c}}_{\text{IUI}}^T)}_{q = \Pr\{\hat{s}_0=0 | s_0=1\}} \\ + \frac{1}{2} \frac{1}{N_{\text{IUI}}} \sum_{\mathbf{s}_{\text{IUI}} \in \mathcal{M}} \underbrace{(1 - Q(\xi, \mathbf{s}_{\text{IUI}} \bar{\mathbf{c}}_{\text{IUI}}^T))}_{p = \Pr\{\hat{s}_0=1 | s_0=0\}}, \quad (12)$$

where $Q(a, b)$, q , and p denote the regularized Gamma function, the error probability for $s_0 = 1$, and the error probability for $s_0 = 0$, respectively.

PROOF. P_e can be derived as follows:

$$P_e \stackrel{(a)}{=} \frac{1}{N_{\text{IUI}}} \sum_{\mathbf{s}_{\text{IUI}} \in \mathcal{M}} \left(\frac{1}{2} \Pr\{r < \xi | \mathbf{s}_{\text{IUI}}, s_0 = 1\} \right. \\ \left. + \frac{1}{2} \Pr\{r \geq \xi | \mathbf{s}_{\text{IUI}}, s_0 = 0\} \right) \\ \stackrel{(b)}{=} \frac{1}{N_{\text{IUI}}} \sum_{\mathbf{s}_{\text{IUI}} \in \mathcal{M}} \left(\frac{1}{2} \sum_{r=0}^{\xi-1} \frac{(\bar{c}_s + \mathbf{s}_{\text{IUI}} \bar{\mathbf{c}}_{\text{IUI}}^T)^r e^{-(\bar{c}_s + \mathbf{s}_{\text{IUI}} \bar{\mathbf{c}}_{\text{IUI}}^T)}}{r!} \right. \\ \left. + \frac{1}{2} \left(1 - \sum_{r=0}^{\xi-1} \frac{(\mathbf{s}_{\text{IUI}} \bar{\mathbf{c}}_{\text{IUI}}^T)^r e^{-(\mathbf{s}_{\text{IUI}} \bar{\mathbf{c}}_{\text{IUI}}^T)}}{r!} \right) \right), \quad (13)$$

where we exploit in (a) the threshold detection rule (9), in (b) the fact that r is Poisson distributed, and finally the cumulated density function (CDF) of a Poisson distribution $\sum_{k=0}^{x-1} \frac{(\lambda)^k e^{-\lambda}}{k!} = \frac{\Gamma(x, \lambda)}{\Gamma(x)} = Q(x, \lambda)$, with $x > 0$ to obtain (12). Here, $\Gamma(a, b)$, $\Gamma(a)$, and $\frac{\Gamma(a, b)}{\Gamma(a)} = Q(a, b)$ denote the upper incomplete Gamma function, the Gamma function, and the regularized Gamma function, respectively. \square

4.3 Area Rate Efficiency of MC Systems

Now, we provide the achievable information transmission rate of an individual transmission link, the spatial multiplexing rate, and finally the ARE which involves both aforementioned rates.

4.3.1 User Rate. As the transmission is binary, i.e., $s_0, \hat{s}_0 \in \{0, 1\}$, we model the point-to-point transmission link as a binary channel with achievable data rate [10, eq. (9.7)]

$$R_{\text{SISO}} = I(s_0; \hat{s}_0) = H(\hat{s}_0) - H(\hat{s}_0 | s_0), \quad (14)$$

which we refer to as user rate. Here, $s_0, \hat{s}_0, I(\cdot; \cdot)$, and $H(\cdot)$ denote the channel input, the channel output, the mutual information, and the entropy function, respectively, where $H(\hat{s}_0) = -\frac{1}{2}((1-p+q) \log_2(\frac{1}{2}(1-p+q)) + (1-q+p) \log_2(\frac{1}{2}(1-q+p)))$ [10, eq. (2.35)] and $H(\hat{s}_0 | s_0) = -\frac{1}{2}((1-p) \log_2(1-p) + p \log_2(p) +$

$q \log_2(q) + (1-q) \log_2(1-q))$ [10, eq. (8.4)]. Two extreme cases of the binary channel are the Z-Channel and the Binary Symmetric Channel (BSC) [10]. A Z-Channel is characterized by error-free transmission for $s_0 = 0$, i.e., $p = 0$, and possible errors for $s_0 = 1$ and is an appropriate approximation, when the IUI approaches zero. On the other hand, for large IUI, the difference between the two possible transmission errors p and q approaches zero. Hence, the BSC, which assumes $p = q$, accurately approximates the binary channel for cases where r in (1) is dominated by IUI. We note that in a BSC the mutual information [10] is maximized by equiprobable binary input and (14) simplifies to the channel capacity of a BSC, i.e., $R_{\text{SISO}} = C_{\text{BSC}} = [1 - H_b(P_e)]$ [10]. Here, $H_b(P_e)$ denotes the binary entropy function for a given error probability $P_e = p = q$, c.f. (12). However, to ensure the accuracy for all levels of IUI, we employ (14) for our analysis in Section 5.

4.3.2 Spatial Multiplexing Rate. We define the spatial multiplexing rate as the number of transmission links per unit of space, i.e., $R_{\text{loc}} = \frac{1}{A_{\text{cell}}}$ with unit [$1/\text{m}^2$], where A_{cell} is the area reserved for one TX-RX pair, i.e., one hexagon. Note that the smaller A_{cell} , the higher the spatial multiplexing rate.

4.3.3 Area Rate Efficiency. We define the ARE based on R_{SISO} and R_{loc} as follows

$$R_{\text{eff}} = R_{\text{SISO}} R_{\text{loc}} = \frac{1}{A_{\text{cell}}} [H(\hat{s}_0) - H(\hat{s}_0 | s_0)] \quad (15)$$

with unit [bit/m^2]. Note that the two rates, R_{SISO} and R_{loc} , have different dependencies on the density of the TXs and RXs in the system. In particular, increasing the density of the TX-RX pairs increases R_{loc} , but decreases R_{SISO} as the BER increases, and vice versa. Hence, the ARE comprises the single link performance in terms of R_{SISO} and the area usage efficiency in terms of R_{loc} , and therefore provides a useful performance metric to gain insight into how efficiently given TX and RX areas are exploited for maximization of the overall information transmission of a system.

5 PERFORMANCE EVALUATION

In this section, we first explain the simulation setup. Then, we evaluate the analytical expression for the CIR in (2) and compare it to results from particle-based simulation (PBS). Finally, the analytical expressions for the BER and the ARE are evaluated.

5.1 Choice of Parameters, Particle-Based Simulation, and Monte Carlo Simulation

The default values of the channel parameters are given in Table 1. For the computation of the CIR, the infinite sum in (2) was truncated to 21 terms, i.e., $k_{\text{max}} = 20$. Furthermore, the threshold value ξ in (10) and the BER in (12) were computed for a truncated number of interferers, namely $N_{\text{TX}} - 1 = 36$. The chosen numbers of interferers correspond to the first three rings within the hexagonal grid shown in Fig. 2.

5.1.1 Monte Carlo Simulation. To verify the analytical expressions and to show that limiting the number of interferers for numerical evaluation does not affect accuracy, we used Monte Carlo simulation. For Monte Carlo simulation, we considered $N_{\text{TX}} - 1 = 1260$ interferers. First, we randomly generated $I = 10^5$ realizations of possible transmit symbol vectors $\mathbf{s}_{\text{all}} = [s_0, \mathbf{s}_{\text{IUI}}]$. Then, we generated the number of molecules observed at RX_0 based on the

Table 1: Default Parameter Values Used.

Variable	Definition	Value
c	Cell centers distance	$[5 \cdot 10^{-2}, 5]$ [m]
S_{RX}	Receiver radius (neighboring receivers touch each other)	$\frac{c}{2}$ [m]
L_{RX}	Receiver length	0.2 [m]
V_{RX}	Receiver volume	$S_{RX}^2 \pi L_{RX}$ [m ³]
d	Distance between planes	0.5 [m]
v	Flow velocity	0.2 [m/s]
D	Diffusion coefficient	0.01 [m ² /s]
N_m	Number of released molecules	100
Δt	Time resolution PBS & Monte Carlo Simulation	10^{-3} [s]
T_{sim}	Simulation length	15 [s]

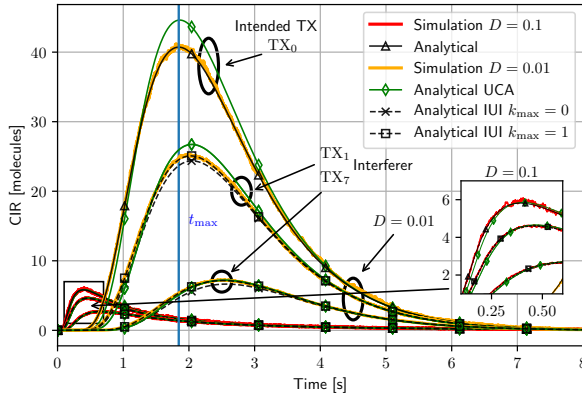


Figure 3: CIR for TX₀, TX₁, and TX₇ with $c = 0.2$ for different diffusion coefficients D . The proposed analytical results are shown with markers and are compared to results from PBS.

channel model in (1), where RVs c_s and c_{IUI} were modelled as Poisson distributed according to (5) and (6). Parameters \bar{c}_s and \bar{c}_{IUI} were obtained from the CIR in (2). Next, (12) was numerically evaluated, i.e., the BER was computed for all possible threshold values up to 200, i.e., $\xi \leq 200$, and the lowest BER together with the corresponding threshold value and error probabilities p and q were selected.

5.1.2 Particle-Based Simulation. To verify the accuracy of the analytical expressions for the CIR in (2), 3-D stochastic particle-based computer simulations were carried out. The results from PBS were averaged over 3000 realizations.

5.2 Verification of CIR

Fig. 3 shows the CIR obtained from the proposed analytical expression (2) (black color) and PBS (yellow and red color) as ground truth. Results for the truncation of the sum in (2) to 1 and 2 terms, i.e., $k_{max} = 0$ and $k_{max} = 1$, are depicted with dashed lines. Furthermore, we show results for a CIR obtained based on the uniform concentration assumption (UCA) at the RX (green color), where the molecule concentration at the center of the RX is scaled with the volume of the RX instead of integrating the concentration over the RX volume, i.e., $CIR_{UCA,i} = C(x_{RX}, x_{0,i}, y_{RX}, y_{0,i}, z_{RX}, z_{0,i}, t, t_{0,i})V_{RX}$

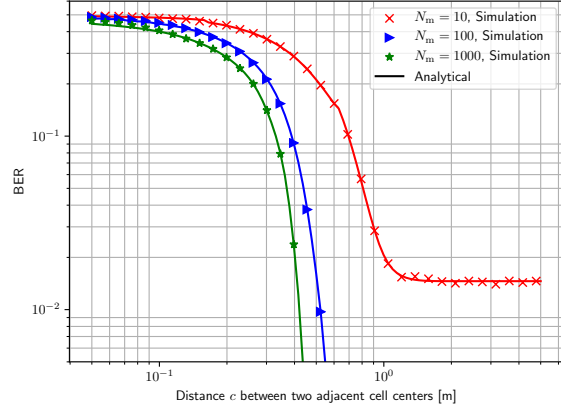


Figure 4: BER as a function of cell center distance c for different numbers of released molecules N_m . The results from Monte Carlo simulation are depicted by markers.

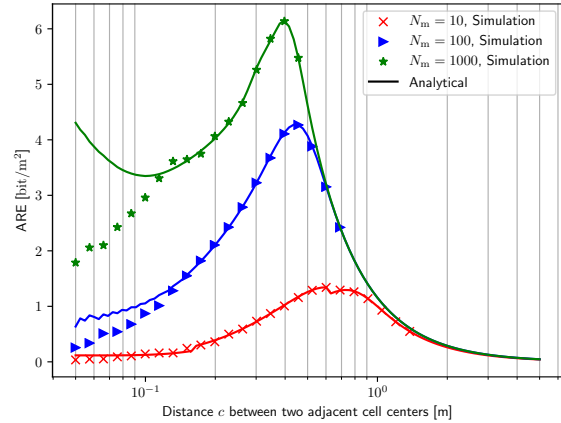


Figure 5: ARE as a function of cell center distance c for different numbers of released molecules N_m . The results from Monte Carlo simulation are depicted by markers.

[8]. The sampling time t_s is denoted by t_{max} (blue color). The verification of the CIR is exemplarily done for TX₀, TX₁, and TX₇ for a grid with cell-center distance $c = 0.2$, see Fig. 2, and two different diffusion coefficients D .

We first concentrate on the CIRs for diffusion coefficient $D = 0.01$. From Fig. 3, we observe that for the desired transmitter TX₀, the proposed CIR is in excellent agreement with the PBS results (yellow color). Note that the sum in (2) simplifies for TX₀ to the term $\gamma(1, \frac{S_{RX}^2}{4Dt})$ as $r_{0,0}^2 = 0$ for TX₀. For TX₁ and TX₇ the proposed model in (2) matches the PBS result not yet for $k_{max} = 0$, but for $k_{max} = 1$, i.e., for truncating the infinite sum to two terms. The CIR based on the UCA deviates from the PBS result, especially for TX₀ and TX₁. The CIR expression for the UCA is in general simpler, but less precise. The aforementioned observations are also valid for the CIRs for $D = 0.1$. Therefore, we conclude that the derived expression for the CIR in (2) is accurate. Note that it is sufficient to truncate the infinite sum in (2) after two terms for the parameters considered in Fig. 3. However, we use $k_{max} = 20$ for our analysis in Section 5.3.

5.3 Evaluation of BER and ARE

In Figs. 4 and 5, BER and ARE are shown as functions of the hexagonal cell center distance c for different numbers of released molecules N_m . Fig. 4 shows that for small c , when the TXs are closely spaced, the BER approaches 0.5 because of the excessive interference. We observe that increasing c decreases the BER and, for large values of c , the IUI approaches zero and the BER reaches a constant error floor. For the range of BER values shown in Fig. 4, the error floor is visible only for $N_m = 10$, but also occurs for larger N_m at lower BER values. In particular, in the absence of IUI, the optimal detection threshold equals one, i.e., $\xi = 1$, and detection errors can only occur for $s_0 = 1$. The corresponding error probability q in (12) is characterized by the probability of receiving zero molecules at RX_0 although N_m molecules were released by TX_0 . In particular, for large values of c , RX_0 spans a large area of the RX-plane as S_{RX} scales with c . Therefore, the error probability is constant and approximately inversely proportional to the probability of at least one molecule reaching the RX. Furthermore, Fig. 4 shows that the BER decreases for increasing N_m . We observe that the difference in BER for different N_m decreases for smaller cell distances c .

Fig. 5 shows that the ARE has a unique maximum and we denote the corresponding cell center distance as c^{opt} . We observe that both, decreasing and increasing c compared to c^{opt} , decreases the ARE asymptotically towards $ARE \rightarrow 0$. For small c , the considered system is dominated by excessive IUI, i.e., the small R_{SISO} dominates the ARE (15). However, for large c , the system's usage of the spatial resource is not optimal, as the hexagonal cell area reserved for one TX-RX link is large, i.e., the small R_{loc} dominates the ARE (15). From the existence of a maximum ARE, we conclude that there exists an optimal TX-RX link density, which is achieved by TX positions with cell center distance $c = c^{opt}$. Next, we focus on the impact of the numbers of released molecules N_m . Fig. 5 shows that increasing N_m also increases the peak value of the ARE. We observe that c^{opt} is smaller for larger numbers of released molecules N_m , i.e., the optimal density of the independent users is larger for larger N_m . We note that, in practical applications, there might be an upper limit on N_m due to limited resources. We further observe small ripples in the ARE for $N_m = 10$ and $N_m = 100$ which are caused by the fact that threshold ξ is limited to integer values. Finally, we observe, that the analytical solution deviates from the Monte Carlo simulation result for small c . The reason for this is that for small c , more than 36 interferers have to be considered in order to properly model the IUI. In fact, the actual number of interferers needed to accurately approximate the system behavior increases with decreasing c and should be chosen carefully.

6 CONCLUSION

In this paper, we focused on the spatial dimension of MC systems. We considered a 3-D system with multiple independent and spatially distributed point-to-point transmission links, where the TXs and the RXs were positioned according to a regular hexagonal pattern, respectively. We developed an analytical expression for the CIRs of all existing TX-RX links. We further applied threshold-based detection and analyzed the BER of a single transmission link. The corresponding detection threshold was derived taking into account the statistics of the MC channel and the statistics of the IUI. Next, we proposed the ARE as a new performance metric for MC

systems to characterize how efficiently given TX and RX areas are used for information transmission. The ARE reflects the impact of the user density, i.e., the number of TXs and RXs per unit area, and the IUI dependent performance of each individual transmission link on the overall performance of the MC system. Finally, quantitative results for the optimal user density for maximization of the ARE of MC systems were provided.

The ARE analyzed in this paper provides a new perspective for designing multiuser MC systems. Although we have considered a particular multiuser MC setup, the concept to analyze the system performance in terms of the ARE can be extended to other MC systems, including different MC channels, different TX and RX grids, and different types of TXs and RXs.

REFERENCES

- [1] Milton Abramowitz and Irene A Stegun. 1972. *Handbook of Mathematical Functions with Formulas, Graphs, and Mathematical Tables*. Vol. 55. US Government Printing Office.
- [2] J. G. Andrews, F. Baccelli, and R. K. Ganti. 2011. A Tractable Approach to Coverage and Rate in Cellular Networks. *IEEE Trans. Commun.* 59, 11 (Nov. 2011), 3122–3134. <https://doi.org/10.1109/TCOMM.2011.100411.100541>
- [3] M. Damrath, H. B. Yilmaz, C. Chae, and P. A. Hoeher. 2018. Array Gain Analysis in Molecular MIMO Communications. *IEEE Access* 6 (Oct. 2018), 61091–61102. <https://doi.org/10.1109/ACCESS.2018.2875925>
- [4] Y. Deng, A. Noel, W. Guo, A. Nallanathan, and M. El-kashlan. 2017. Analyzing Large-Scale Multiuser Molecular Communication via 3-D Stochastic Geometry. *IEEE Trans. Mol. Biol. Multi-Scale Commun.* 3, 2 (June 2017), 118–133. <https://doi.org/10.1109/TMBMC.2017.2750145>
- [5] Nariman Farsad, H. Birkan Yilmaz, Andrew Eckford, Chan-Byoung Chae, and Weisi Guo. 2016. A Comprehensive Survey of Recent Advancements in Molecular Communication. *IEEE Commun. Surveys Tuts.* 18, 3 (July 2016), 1887–1919. <https://doi.org/10.1109/COMST.2016.2527741>
- [6] M. C. Gursoy, E. Basar, A. E. Pusane, and T. Tugcu. 2019. Index Modulation for Molecular Communication via Diffusion Systems. *IEEE Trans. Commun.* 67, 5 (May 2019), 3337–3350. <https://doi.org/10.1109/TCOMM.2019.2898665>
- [7] Y. Huang, M. Wen, L. L. Yang, C. B. Chae, and F. Ji. 2019. Spatial Modulation for Molecular Communication. *IEEE Trans. Nanobiosci.* 18, 3 (July 2019), 381–395. <https://doi.org/10.1109/TNB.2019.2905254>
- [8] V. Jamali, A. Ahmadzadeh, W. Wicke, A. Noel, and R. Schober. 2019. Channel Modeling for Diffusive Molecular Communication—A Tutorial Review. *Proc. IEEE* 107, 7 (July 2019), 1256–1301. <https://doi.org/10.1109/JPROC.2019.2919455>
- [9] V. Jamali, Nariman Farsad, R. Schober, and A. Goldsmith. 2018. Non-Coherent Detection for Diffusive Molecular Communication Systems. *IEEE Trans. Commun.* 66 (June 2018), 2515–2531. <https://doi.org/10.1109/TCOMM.2018.2792457>
- [10] David JC MacKay. 2003. *Information Theory, Inference and Learning Algorithms* (1 ed.). Cambridge University Press, Cambridge.
- [11] L. Meng, P. Yeh, K. Chen, and I. F. Akyildiz. 2012. MIMO communications based on molecular diffusion. In *Proc. IEEE Global Commun. Conf. (GLOBECOM)*, 5380–5385. <https://doi.org/10.1109/GLOCOM.2012.6503976>
- [12] R. Nasri and A. Jaziri. 2016. Analytical Tractability of Hexagonal Network Model With Random User Location. *IEEE Trans. Wireless Commun.* 15, 5 (May 2016), 3768–3780. <https://doi.org/10.1109/TWC.2016.2528245>
- [13] A. Noel, K. C. Cheung, and R. Schober. 2014. Improving Receiver Performance of Diffusive Molecular Communication With Enzymes. *IEEE Trans. Nanobiosci.* 13, 1 (March 2014), 31–43. <https://doi.org/10.1109/TNB.2013.2295546>
- [14] A. Noel, K. C. Cheung, and R. Schober. 2014. A Unifying Model for External Noise Sources and ISI in Diffusive Molecular Communication. *IEEE J. Sel. Areas Commun.* 32, 12 (Dec. 2014), 2330–2343. <https://doi.org/10.1109/JSAC.2014.2367693>
- [15] S. M. R. Rouzgar and U. Spagnolini. 2019. Diffusive MIMO Molecular Communications: Channel Estimation, Equalization, and Detection. *IEEE Trans. Commun.* 67, 7 (July 2019), 4872–4884. <https://doi.org/10.1109/TCOMM.2019.2910252>
- [16] B. Tepekule, A. E. Pusane, H. B. Yilmaz, C. Chae, and T. Tugcu. 2015. ISI Mitigation Techniques in Molecular Communication. *IEEE Trans. Mol. Biol. Multi-Scale Commun.* 1, 2 (June 2015), 202–216. <https://doi.org/10.1109/TMBMC.2015.2501745>